drones

MDPI

Article

Large-Scale Earthwork Progress Digitalization Practices Using Series of 3D Models Generated from UAS Images

Jin-Woo Cho [1], Jae-Kang Lee [1,*] and Jisoo Park [2]

[1] Korea Institute of Civil Engineering and Building Technology, Goyang 10223, Korea; jinucho@kict.re.kr
[2] School of Civil and Environmental Engineering, Georgia Institute of Technology, Atlanta, GA 30332, USA; jpark711@gatech.edu
* Correspondence: jaekang.lee@kict.re.kr; Tel.: +82-31-910-0753

Abstract: Since the Fourth Industrial Revolution, existing manpower-centric manufacture has been shifting towards technology and data-centric production in all areas of society. The construction sector is also facing a new paradigm called smart construction with a clear purpose of improving productivity and securing safety by applying site management using information and communications technology (ICT). This study aims to develop a framework for earthwork process digitalization based on images acquired by using the unmanned aerial system (UAS). The entire framework includes precise UAS data acquisition, cut-and-fill volume estimation, cross-section drawing, and geo-fencing generation. To this end, homogeneous time-series drone image data were obtained from active road construction sites under earthwork. The developed system was able to generate precise 3D topographical models and estimate cut-and-fill volume changes. In addition, the proposed framework generated cross-sectional views of each area of interest throughout the construction stages and finally created geo-fencing to assist the safe operation of heavy equipment. We expect that the proposed framework can contribute to smart construction areas by automating the process of digitizing earthwork progress.

Keywords: UAS (Unmanned Aerial Systems); earthwork; volume estimation; point cloud; construction management; drones

Citation: Cho, J.-W.; Lee, J.-K.; Park, J. Large-Scale Earthwork Progress Digitalization Practices Using Series of 3D Models Generated from UAS Images. *Drones* **2021**, *5*, 147. https://doi.org/10.3390/drones5040147

Academic Editor: Sungjin Kim

Received: 11 November 2021
Accepted: 10 December 2021
Published: 12 December 2021

1. Introduction

Many technologically advanced countries are attempting to expand and apply information and communications technology (ICT) to the construction sector. Most nations consider this objective as a national agenda. For example, the South Korean government has presented a vision of "Smart Construction 2025" for technological innovation in the construction sector and announced the "Roadmap for Smart Construction Technology". The South Korean government is promoting various policies and projects based on cutting-edge technology to create opportunities for the construction industry to take a leap forward. Generally, smart construction is defined as a method that innovatively enhances construction productivity and safety by combining smart construction technology with traditional construction methods [1]. The main technologies for smart construction include unmanned aerial systems (UAS), building information modeling (BIM), augmented/virtual reality (AR/VT), the internet of things (IoT), Big Data, etc. [2]. These are the critical technologies for each stage of the construction process, such as design, construction, and maintenance.

The earthworks for road and building complex construction are the optimal construction process to which these technologies supporting smart construction can be applied. Both the private and public sectors have shown great interest and demand in the development of a digital platform for comprehensive management of earthworks based on data (soil movement and loading) and monitoring technology that can automatically manage the quality of each construction process. Therefore, various methodologies have been proposed for the systematic management of earthworks in road construction. Studies such

as automation of earthmoving equipment [3,4], the control system for optimal equipment operation [5–7], and digital platform for earthwork sites [8] are the representative fundamental research studies. In order to automate and digitize such earthwork sites, it is necessary to collect, monitor, analyze, predict, and share various data of the construction site. In addition, technology that can accurately and quickly monitor changed topography information and construction progress at the earthwork site is required. In the past, ground survey equipment such as the total station was primarily used to acquire the topographic information at earthworks sites. However, the occurrence of shaded areas due to obstacles, such as mountainous terrain and excessive workforce and time required to acquire field information, has been pointed out as a problem with the total station. Recently, UASs have received attention as a key method that can monitor site information quickly and accurately.

Although drones are moving objects that are very sensitive to the weather environment, they can easily observe a large area periodically [9]. In addition, UAS has the advantage of quickly judging the standards of image quality set in advance and responding at the site. UASs have higher efficiency than conventional surveying methods in terms of convenient operation, promptness, and economics [10]. These image data can be used for construction change detection, progress monitoring, and digital documentation. Moreover, if an appropriate number of ground control points (GCPs) for georeferencing are secured, generating highly accurate digital surface models (DSM) and 3D point clouds is possible [11,12]. The DSMs and 3D point clouds can be applied to cut-and-fill volume estimation [13]. It is deemed that these advantages are able to contribute significantly to periodic, systematic, and data-based construction process management proposed in this study.

Based on the advantages of UAS, this study aims to develop an all-in-one framework for earthwork digitalization using UAS images. The proposed framework is divided into two main parts. First, standards for UAS operation, image production, and image quality to construct a 3D construction topo-graphic map were proposed. In addition, the second part includes data analysis for construction progress monitoring and digitalization using 3D models.

2. Related Studies

2.1. 3D Construction Topographic Modeling

Conventional methods to create 3D topographic models of construction sites use traditional field survey technologies such as total stations and global navigation satellite systems (GNSS). These surveying devices are still used in many construction fields or infrastructure monitoring areas because they can output accurate global coordinates of measured points [14–16]. However, since this type of surveying technology yields coordinates of a specific point during single surveying, generating a high-density 3D model with them is challenging. In order to address the problems, several researchers employed terrestrial laser scanning (TLS) to generate dense point clouds. Slattery et al. (2012) introduced a method of using TLS for road construction earthwork volume calculation [17]. Williams (2012) compared the 3D positioning accuracy of TLS and mobile laser scanning (MLS) [18]. Although TLS-based modeling technology can create high-density 3D point clouds of earthwork fields, laser scanning of large-scale construction sites takes plenty of time and labor, and the registration process for aligning multiple scans into a single model also requires numerous time and expertise. In particular, since laser scanning in road construction fields where long-strip scanning is required does not allow making a closed-condition for registration, the registration error can be accumulated in the longitudinal direction [19].

Compared to TLS, UAS is a more straightforward solution for generating 3D topographic models of large-scale construction sites. For this reason, various studies on 3D mapping for construction projects using UASs have been presented. Kim et al. (2020) demonstrated a method of construction management using UASs [20]. Park et al. (2018) and Kim et al. (2019) also proposed an automated framework using UAS and mobile

laser scanning robots at the same time to generate 3D models of construction sites [21,22]. They developed an approach to build occlusion-free 3D models by combining 3D models created from UASs and mobile robots. As such, the photogrammetric method based on UAS images has become the most widely used for 3D topographic modeling of large construction sites based on UAS's high usability and efficiency. For this reason, this study also employed 3D topographic models built by sequential UAS images for earthwork progress documentation and digitalization.

2.2. Earthwork Progress Digitalization Using UAS

With the advantages of UAS applications, several researchers have employed UAS applications for earthwork progress monitoring and documentation. Siebert and Teizer (2014) presented the UAS-based 3D topo model generation method. They built a digital elevation model generation (DEM) from sequential UAS images with a photogrammetric technique and visualized cut-and-fill areas. Cho and Park (2019) compared the efficiency of different technologies, such as TLS, MMS, and UAS, in road earthwork construction survey and volume estimation [19]. They identified that UAS is the most effective method for 3D grade control and volume estimation in roadway construction in terms of time and cost for creating 3D dense point clouds. Wang et al. (2017) demonstrated a method for calculating volume from UAS-generated 3D topographic models [23], and Kavaliauskas et al. (2021) presented a BIM-based earthwork quantity estimation using UAS-generated 3D reality mesh models [24]. The aforementioned studies emphasized the efficiency and usability of UASs in large-scale earthwork progress monitoring and volume estimation. However, most studies have calculated the current amount of earthwork by comparing only one model with the design model. Few studies on calculating the amount of earthwork by sequentially comparing a number of models progressively generated over a long period of earthwork progress have been presented. Moreover, although some studies demonstrated a method of creating slope maps with UAS images for the safe operation of ground vehicles in construction sites [25,26], there is a lack of research on drawing geo-fencing generated from UASs for the safe operation of heavy equipment. This study, therefore, introduces actual practices on UAS-based earthwork progress digitalization by using timely generated sequential models of an active earthwork construction site. The practices include the entire process from UAS data acquisition to documentation.

3. Earthwork Progress Digitalization Practices Using UAS

3.1. Overall Framework

This study proposes a framework for earthwork progress digitalization using UAS images, as shown in Figure 1. Although the entire framework is classified into three main stages, (1) time-series 3D topographic model generation, (2) earthwork data analysis and digitalization, and (3) applications, this study only focused on the two stages before applications. In the 3D topo model generation stage, standardized UAS image data collection and evaluation methods are described. In the second stage, earthwork data analysis and digitalization, the first step is to align two 3D models generated at two different periods. After that, the framework creates a height differential map from the aligned two models. Our system calculates cut-and-fill volume, generates cross-section views, and draws geo-fencing simultaneously with the height differential map. The final outcomes of earthwork data analysis can be used for earthwork construction progress monitoring and safe operation of heavy equipment. The details of each process are described in the following sections.

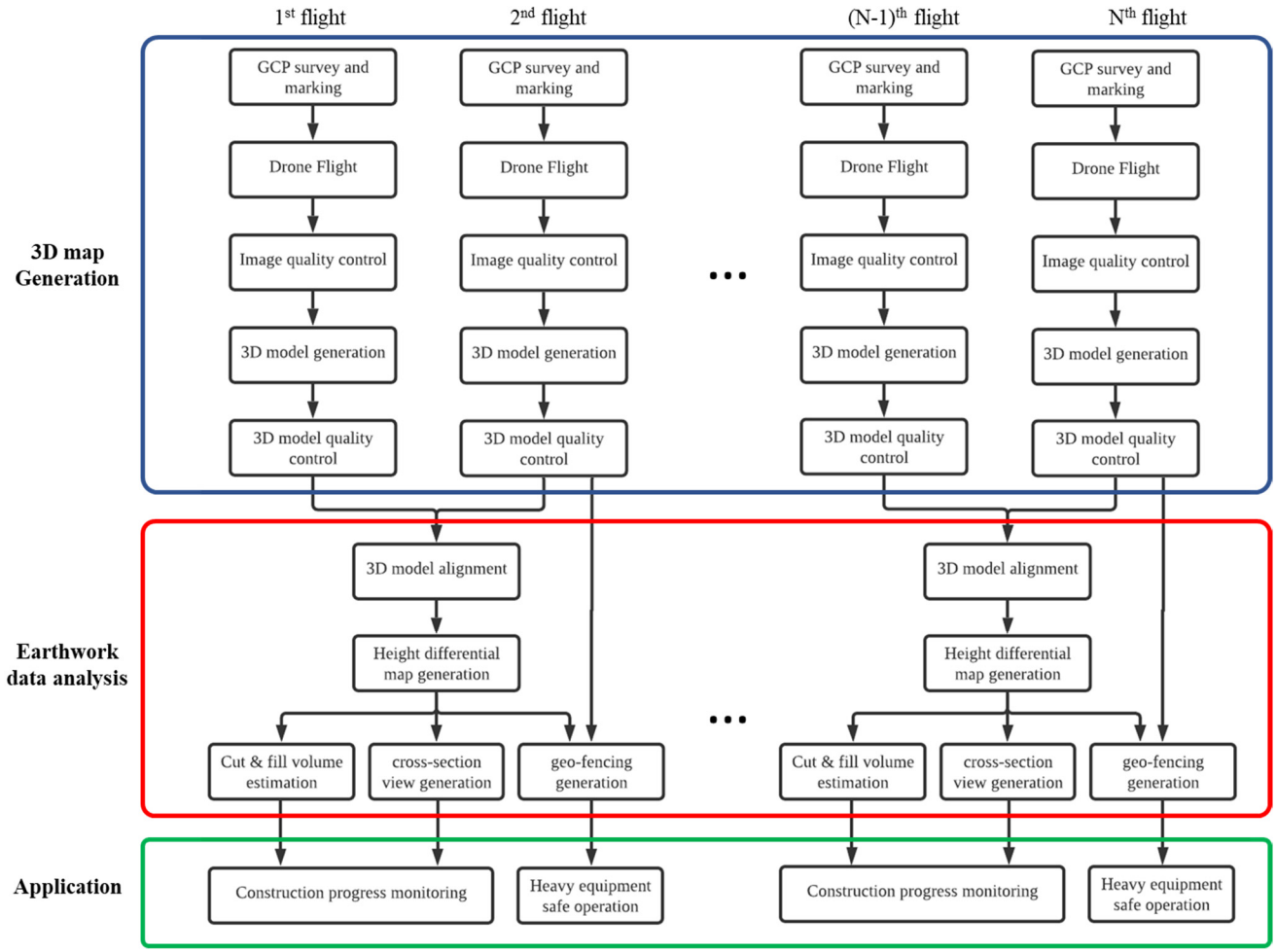

Figure 1. The overall framework for earthwork progress digitalization using UAS images.

3.2. Cartography Using UAS Images for 3D Earthwork Construction Topographic Map

3.2.1. Summary

The first step for earthwork construction process digitalization and documentation is constructing a digital topographic map of the construction site. The construction topographic map built in this study was simultaneously utilized as a base map of the smart earthwork platform. The smart earthwork platform is a platform for digitizing overall earthwork, such as the analysis of compaction performance by compaction equipment. In order for the construction topographic map to be used as the base map of the entire system, high-quality image resolution, timed image production, and positioning accuracy must be satisfied. Furthermore, safety management of the construction site and the consistency of the time-series production drawing in the construction process were considered when producing images. This section covers the standardized procedures for georeferenced UAS image data acquisition, 3D construction topographic map generation, and quality control.

3.2.2. Path Planning and Georeferencing Considering Safety

A highway construction segment of 6.6 km in South Korea was used as a test bed for this study, as shown in Figure 2. UAS image data collection was carried out three times between May and October 2020 at intervals of more than a month to investigate earthwork progress and volume changes. Since 3D construction topography using UAS is used as a basic map of smart earthwork platforms, it is necessary to meet the requirements of high-quality resolution and location accuracy of production drawings. Moreover, since there are many workers and construction equipment at the earthwork site, the flight path

and environmental factors should be reviewed in consideration of their safety. In order to ensure the safety of field workers, a stable rotary-wing type drone capable of vertical take-off and landing (VTOL) must be used, and a battery capacity capable of flying at least 25 min must be ensured. In order to satisfy flight safety and output quality, we used a commercial quadrotor drone, which has a 24-megapixel camera and lithium-ion batteries that can fly for more than 35 min. In addition, the drone was flown only when the wind speed was less than six m/s to increase the safety of the flight. The weight and size of the drone used are 1800 × 1230 × 250 mm and 5.0 kg, and its maximum speed is 50 km/h. We also used Pix4D v.4.5 for photogrammetry. The detailed flight parameters and data processing are described in Table 1.

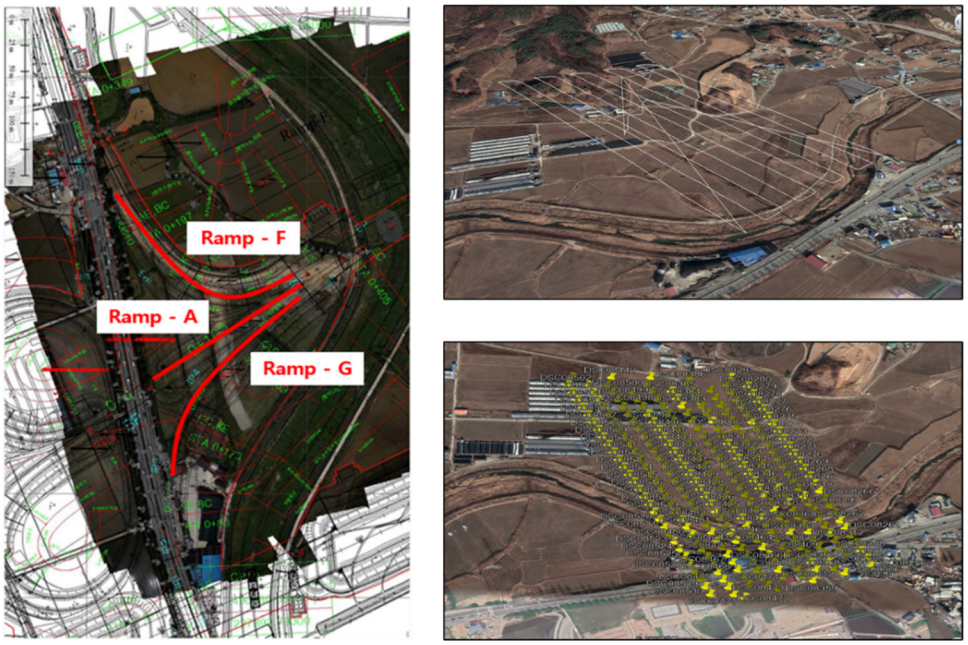

Figure 2. The test field for the UAS image data acquisition.

Table 1. Flight parameters and data processing details.

Categories	Flight Parameter	Categories	Data Processing
Flight height	100 m	# of images	268–281
ISO	400	Image resolution	4000 × 6000 px
Shutter speeds	1/1250 s	CPU	AMD 3.60 GHz
Flight time	25 min	GPU	NVDIA RTX 2060
Overlapping (HTZL/VERT)	75%/80%	Processing time	2.5 h

Before deploying UAS, several reference points called GCP and checkpoint (CP) were measured in advance. RTK-GPS was used to obtain GCP coordinates, and an average of ten observation values for each GCP was finally collected. In fact, there is no regulated tolerance for earthwork volume estimation. Nevertheless, the accuracy and precision of the model are critical in calculating the amount of earthwork, which is in contrast to measurement range and processing speed being more important than the accuracy of the model for change measurement of disaster areas [27–29]. For this reason, we internally set up a tolerable positioning error and image resolution requirement of 3 cm. Figure 3 shows an example of the target for photogrammetry and a scene of acquiring the coordinates at the site. Two of seven GCPs were installed outside the main road construction area so that they could be used continuously during the entire earthwork process.

Figure 3. GCP surveying. (**a**) is the ground target, (**b**) is the GPS surveying for the GCP, and (**c**) is the location of GCPs.

3.2.3. 3D Topographic Model Generation and Evaluation

Figure 4 depicts ortho-images and DSMs (Digital Surface Model) produced from UAS images taken at three different times. In general, two factors (positioning accuracy and image resolution) are considered for maintaining homogeneous image quality. Positioning accuracy is checked by comparing the coordinates of the checkpoint in the image and the actual measurement. Table 2 shows the accuracy of the coordinates for the checkpoints and GCPs in three ortho-images. Although seven GCPs and two CPs were installed at each round, this paper shows the positioning results of two representative GCPs and two CPs. For the GCPs, it was confirmed that the accuracy of the coordinates was within 1~2 cm for all points except for one. Moreover, the accuracy of the checkpoint was about 1~3 cm, which verified that 3D positioning was well performed. For the GCP survey and evaluation, the Geodetic Reference System 1980 (GRS80) reference system and UTM-K coordinate system were used.

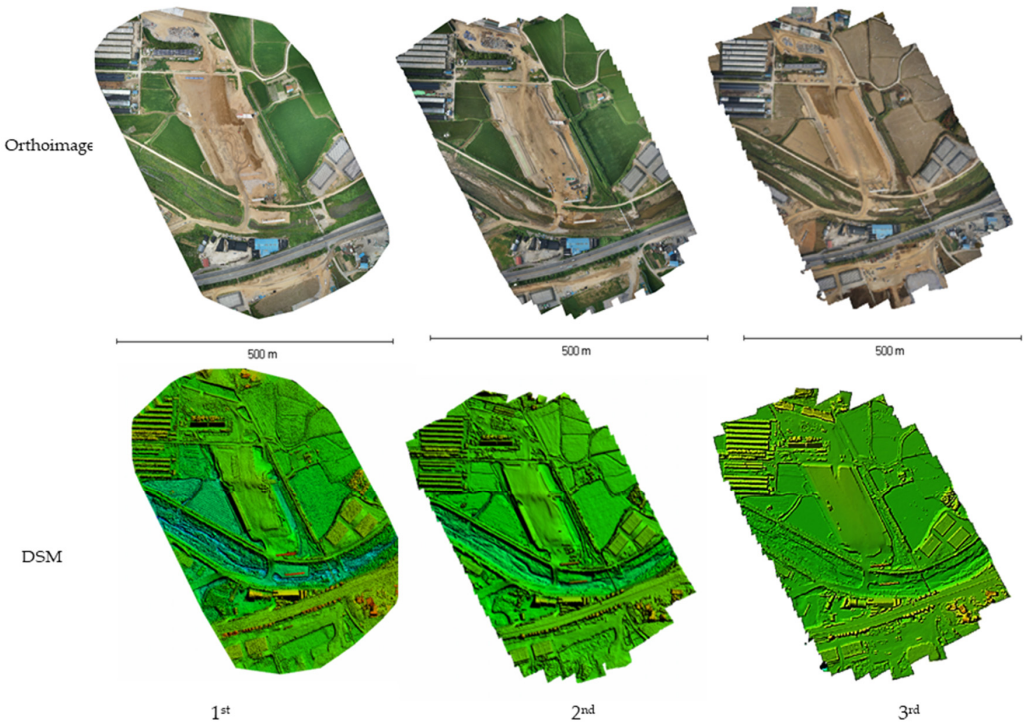

Figure 4. Ortho-image and DSM for each round.

Table 2. Positioning accuracy analysis using GCPs and CPs (GRS80 and UTM-K).

Round	# of GCP #	ΔX (m)	ΔY (m)	ΔZ (m)	ΔXY (m)	Total Error (m)
1st	7	0.004	0.006	0.006	0.007	0.009
2nd	7	0.007	0.012	0.014	0.014	0.020
3rd	7	0.008	0.010	0.010	0.013	0.016
Round	**CP #**	**ΔX (m)**	**ΔY (m)**	**ΔZ (m)**	**ΔXY (m)**	**Total Error (m)**
1st	1	0.009	0.004	0.022	0.010	0.024
	2	0.028	0.010	0.024	0.030	0.038
2nd	1	0.029	0.008	0.003	0.030	0.030
	2	0.012	0.016	0.037	0.02	0.042
3rd	1	0.012	0.005	0.030	0.013	0.033
	2	0.004	0.025	0.007	0.025	0.026

The spatial resolution of images is one of the most crucial sensor quality assessment factors [30]. In order to estimate spatial resolution, we adopted a bar target with 14 levels [31] and the Siemens start targets [32], as shown in Figure 5. These targets provide the level of image resolution by using performance evaluation of geometric features in the marks. The purpose of bar targets is to calculate spatial frequency according to perceivable bar size based on mathematical principles. The size of the largest bar (No. 1) is 1 m × 0.2 m, and the size of bars decreases by 12% sequentially. Spatial frequency using the bar target can be calculated from ground sampling distance (GSD) and minimum width of visible bars, and it is described by the following.

$$\text{Spatial Frequency} = \frac{GSD\ (cm/pixel)}{width\ of\ black\ and\ white\ line\ pairs}, \quad (1)$$

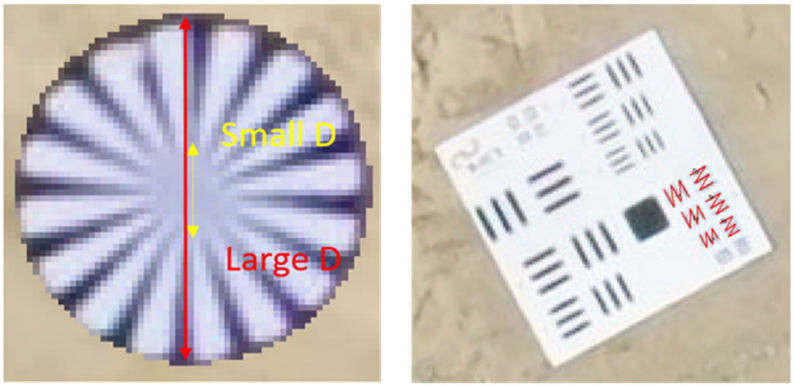

Figure 5. Siemens star target (**a**) and bar target (**b**) displayed in UAS images taken at 100 m above ground level.

This study also employed the Siemens star target, which has a total of 32 black and white lines arranged at regular distances and a radiation angle of 11.25 from the center of the circle. With the Siemens star target, the visual resolution can be measured by the following:

$$l = \frac{\pi \times \frac{d}{D}}{n}, \quad (2)$$

where l is the visual resolution, d/D is the small 'd' over large 'D' in Figure 5, and n is the number of bars. Table 3 describes that the image resolution estimated in this study was

about 2.9 cm, which satisfied the internally required image resolution of 3 cm. The finaly generated 3D models are displayed in Figure 6.

Table 3. UAS image resolution verification and analysis.

Siemens Star Categories	**Large D**	**Small d**	**Diameter Ratio**		**Result**
Visual resolution at 100 m altitude	1.02 m	0.267 m	0.261		0.025 m
Bar Target Categories	**No. 7**	**No. 8**	**No. 9**	**No. 10**	**Average**
Spatial resolution at 100 m altitude	Recognized	Recognized	Recognized	Not recognized	0.029 m

Figure 6. 3D construction map for each round: (**a**) the 1st round, (**b**) the 2nd round, and (**c**) the 3rd round.

3.3. Development of Earthwork Progress Digitalization System

This study developed UAS image-based earthwork progress management and digitalization system based on Python computer programming language. Open-source libraries, such as Matplotlib, Open3D [33], and point cloud library (PCL) [34], were actively utilized to implement functions for 3D point cloud data processing. These functions include the following:

1. Importing UAS-generated point clouds;
2. Aligning point clouds;
3. Setting and extracting the area of interest;
4. Estimating cut and fill volume;
5. Generating cross-section views;
6. Drawing geo-fencing.

The detailed explanations and examples of each function are described in the following sections.

3.3.1. Model Alignment

The first step to compute the cut-and-fill volume change in two different point clouds is by finely aligning both point clouds into a single coordinate system. Since the point clouds used in this study are georeferenced by GCPs measured from RTK-GPS, all point clouds were initially aligned in the World Geodetic System (WGS-84), an Earth-centered one geodetic datum. However, the coordinates measured by using GNSS may be shifted as much as 20 cm or more depending on the weather conditions and satellite positional conditions of the measuring day. For this reason, the developed system employs an iterative closest point (ICP) algorithm for fine alignment of shifted models. ICP is an algorithm for finding a transformation matrix to make the difference between two point clouds minimize [35]. Since the ICP algorithm calculates the distance of closest points, our system first extracts unchanged areas in both point clouds and then finds the transformation matrix from the selected areas with ICP. Then, the computed transformation matrix can be applied

to entire point clouds for fine alignment. The rigid transformation for the fine alignment of two point clouds can be expressed by the following:

$$s_j = T^*(m_i) = R^* m_i + t^*, \tag{3}$$

where s_j and m_i are points in the reference point cloud and the merged point cloud, respectively, T^* is the optimal transformation matrix computed from ICP, and R^* and t^* represent the optimal rotation and the optimal translation, respectively. With the finely aligned point cloud, the proposed system generates a height differential map for estimating cut-and-fill volume change.

3.3.2. Volume Estimation

In order to calculate earthwork volume for the road construction site, the developed system generates a height differential map from two finely aligned models, as revealed in Figure 7. The height differential map is a 2D raster map with a grid size of 1 m × 1 m. The average neighbors per cell is about eight points. If a more precise volume estimation is required, a smaller grid size can be considered. The earthwork volume change-estimating function then uses the 2D raster map.

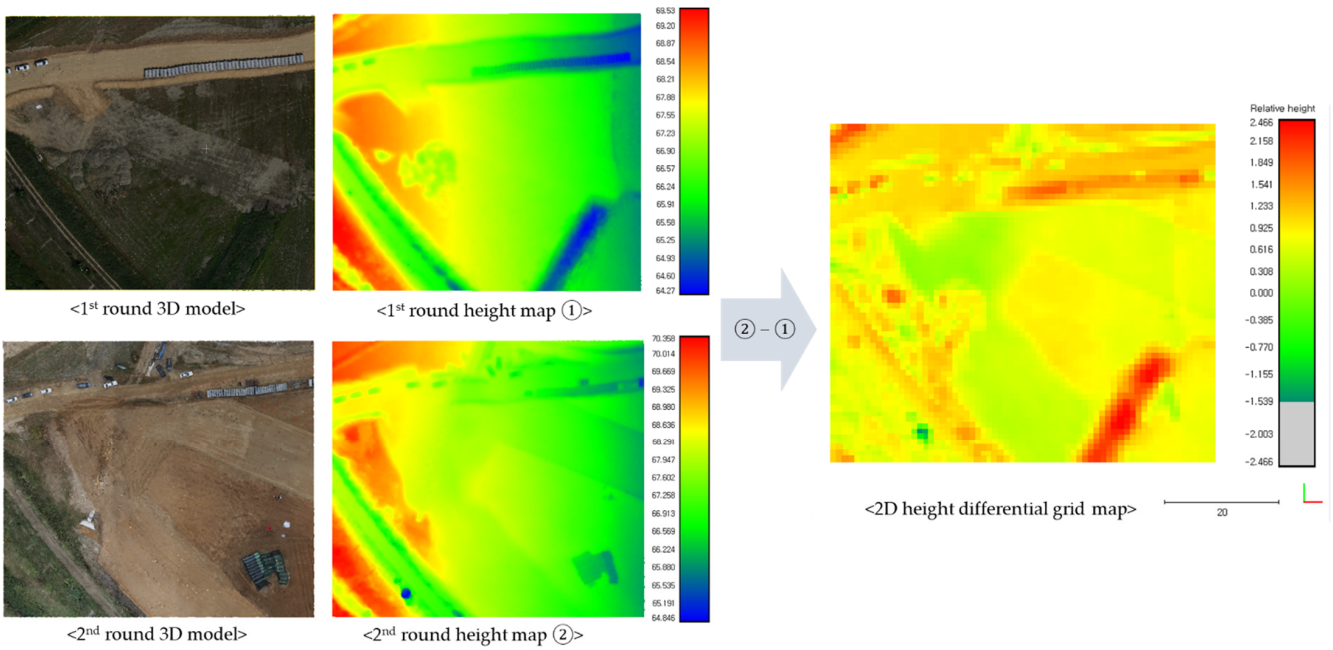

Figure 7. The 2D height differential map generation progress.

The volume estimation function sums up the contribution of each grid. Since this contribution is the volume of the elementary parallelepiped, the volume can be easily calculated by the following:

$$\Delta V = \sum_{i}^{n} \left(x_{grid,i} \times y_{grid,i} \times \Delta H_i \right), \tag{4}$$

where ΔV is the difference of volume summarized in n grids, x_{grid} and y_{grid} are the dimensions of the grids, and ΔH is the height difference in each grid. Empty cells in either the reference and aligned models are filled with height values of the nearest grid.

This study built two height differential maps (Round 2-1 and Round 3-2) to analyze the amount of volume change over time. Figure 8 and Table 4 illustrate analysis results based on the pairs of the topographic models from the first and second rounds and the second and third rounds. The section of road earthwork site where the filling process was

performed the most was set as a comparison area. Based on this analysis, the cut factor, fill factor, area, cut volume, and fill volume were analyzed. The cut factor and fill factor are volume scale factors, and as the models have absolute global coordinates, the scale factors are set as 1.

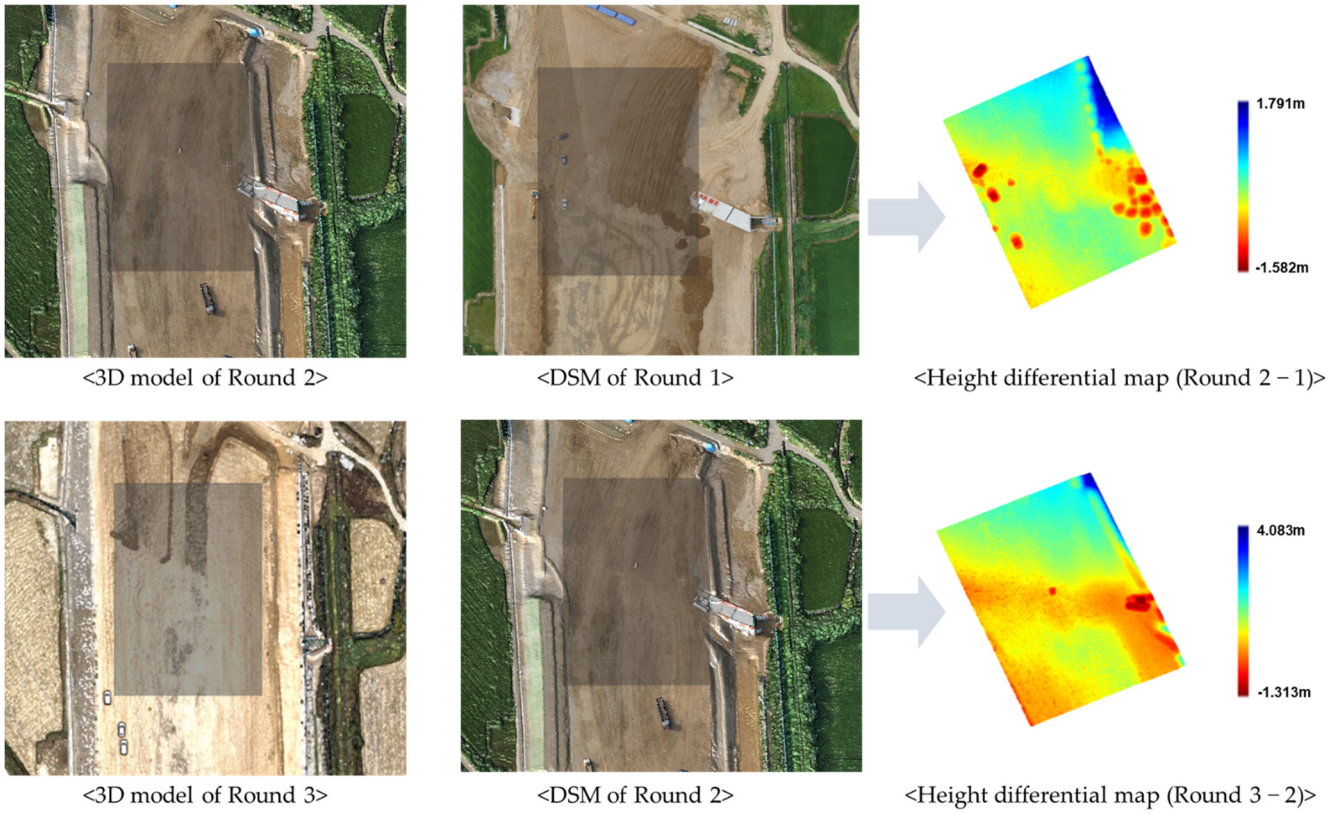

Figure 8. Volume change estimation using height differential maps.

Table 4. Analysis of the volume changes in the topographic maps for rounds 1-2 and 2-3.

Round	Type	Cut Factor	Fill Factor	Area	Cut Volume	Fill Volume	Net Volume
Rounds 2-1	fill	1	1	5035 m^2	161 m^3	757 m^3	596 m^3 <Fill>
Rounds 3-2	fill	1	1	5035 m^2	26 m^3	8738 m^3	8712 m^3 <Fill>

3.3.3. Cross-Section View Generation

The developed earthwork progress digitalization system has a function for generating cross-section views of an area of interest. This function was also implemented by open-source Python libraries, Open3D. This procedure first imports two different 3D point clouds (before earthwork and after earthwork), which are aligned in the previous step, and extracts an area of interest where the user wants to draw cross-section views. Moreover, the user can determine the starting and endpoints of a centerline and the number of sections. The system then divides the line into equal parts according to the given number of sections and finally draws a cross-sectional view at the split sections. By visualizing the layout of the cross-section, the field manager was able to identify the current grade status in the road construction site. Figure 9 illustrates the progress of generating cross-section views from the 3D models of Round 1 and Round 2. In the rightmost figure, the blue lines and orange lines represent the pre-earth elevation (Round 1) and post-earth elevation (Round 2), respectively. The units shown in Figure 9 are all meters.

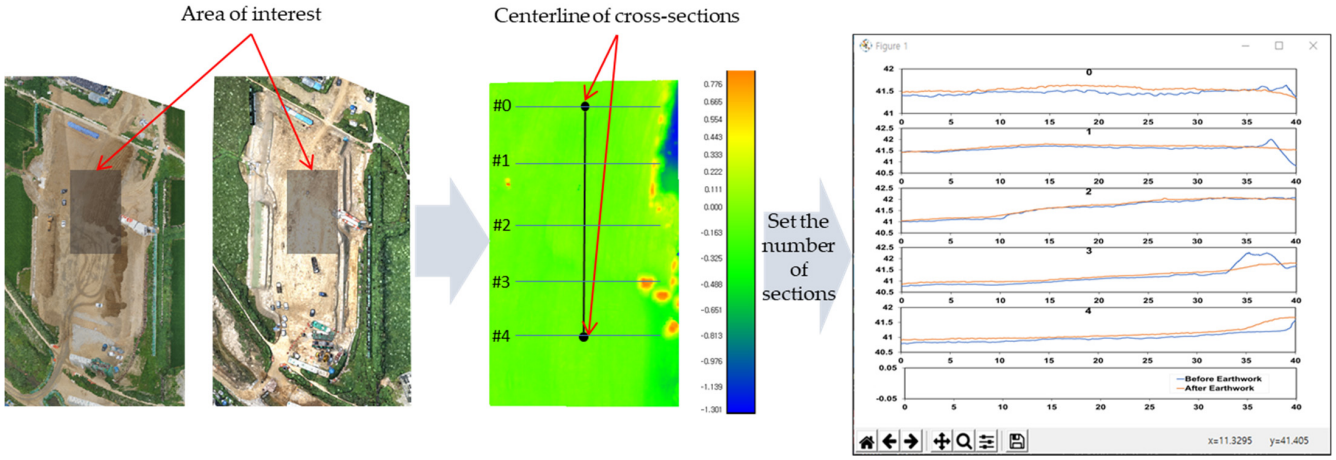

Figure 9. Cross-section views generated from the 3D models of Round 1 and 2.

3.3.4. Geo-Fencing

Geo-fencing, which is a GNSS-enabled technology for creating a virtual boundary or "fence" around a specific location, has been used in the construction field for various purposes, such as the safe operation of heavy equipment and field worker safety management. This study applied geo-fencing to the construction sites to prevent the rollover of heavy equipment during construction and support safe transportation of dumps. Therefore, the geofencing drawing function is mainly divided into two parts: (1) slope-based geofencing and (2) change-based geofencing. Slope-based geofencing can be created by a z-axis point normal vector. The process of estimating normal vectors can be described as follows [34]:

- Find the k number of nearest neighboring points;
- Set the initial normal $\vec{n}_i = \{0, 0, 0\}$;
- Build triangles $T_i = [t_1, t_2, \cdots t_r]$ using points from $\vec{p}_i \cup E_i$ and then compute the corresponding normal vectors $N_i = \left[\vec{n}_1, \vec{n}_2, \cdots, \vec{n}_i\right]$.

For this, the developed system first finds ten nearest neighboring points and then computes the z-axis normal, which can represent the slope angle of each point. After that, a threshold for defining a critical slope angle is determined. The critical slope angle can be defined by the angle causing the rollover of equipment (e.g., 30° for excavator and 15° for crane) [36,37]. Then, our system generates an occupancy map that visualizes the grids with a specific range of z normal values, and the occupancy map is aligned to the original point cloud. As shown in (b) in Figure 10, if the slope angle is over a certain threshold (e.g., 30°), the system makes a geofencing with red color grids in order to prevent certain heavy equipment from passing by that area.

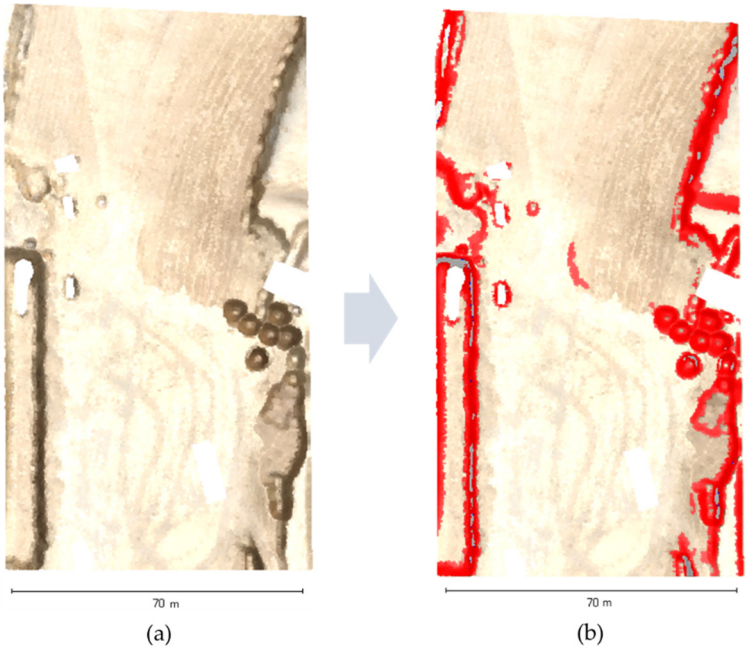

Figure 10. Original 3D model of Round 1 (**a**) and slope-based geo-fencing model (**b**).

In the earthwork construction field, cut-or-filled areas should prevent dump trucks from passing through because those areas may have unstable ground conditions or grading works may not be completed. To this end, we developed a function to draw a geofencing based on the volume change, as shown in Figure 11. This function finds the z-axis normal from the height differential map described in the previous sections to represent the change gradient. Since both slope-based geofencing and change-based geofencing maps have a global coordinate system, they can be easily applied to navigation systems of heavy equipment.

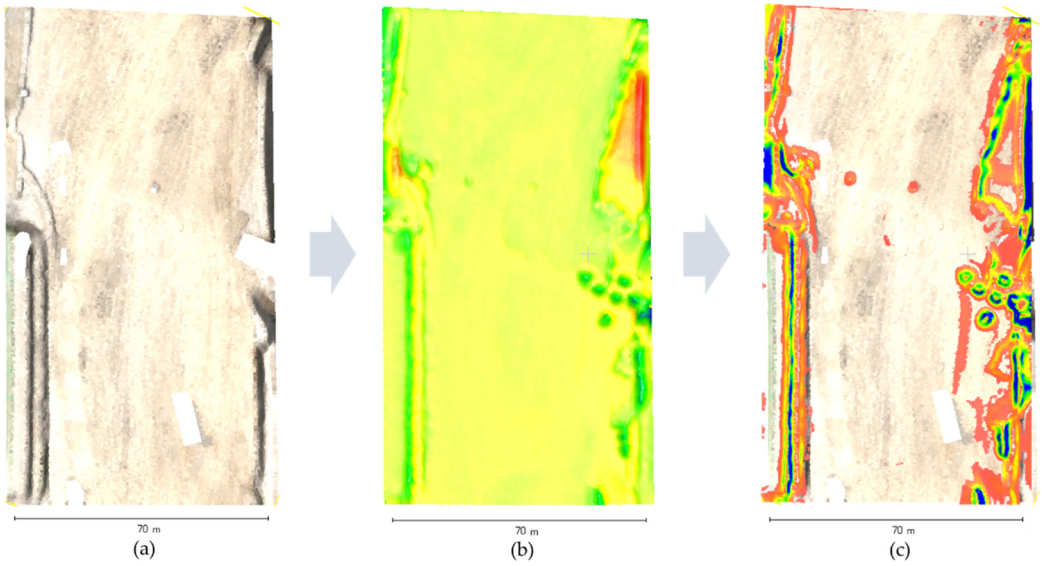

Figure 11. Original 3D model of Round 2 (**a**), height differential map of Round 2-1 (**b**), and volume change-based geo-fencing model (**c**).

4. Discussion

The significant challenge in the visualization of height difference is to eliminate moving objects, such as cars and construction equipment, in the point cloud data. In fact,

the effect of moving objects in volume estimation was not very significant. The differences in volume between the model from which the moving object was removed and the model without removal were 84 m^3 and 72 m^3 in cut and filled, respectively. As a result, the difference in net volumes of the two cases was small. Nevertheless, these objects have a significant effect on creating height differential maps, as shown in Figure 12. Since drone flight must be performed only during the daytime, it is challenging to avoid the influence of moving objects in the construction fields. This study, therefore, erased moving objects in the 3D point cloud manually and filled the empty spots with the nearest neighboring points. Although removing the objects in point cloud data took less than 10 min in this study because there were only a few moving objects, it would be time-consuming if many things that need to be removed were located in the construction sites. In general, the construction sites are congested by various heavy equipment and dump trucks. For this reason, we recognized the need for a method that can remove these objects automatically.

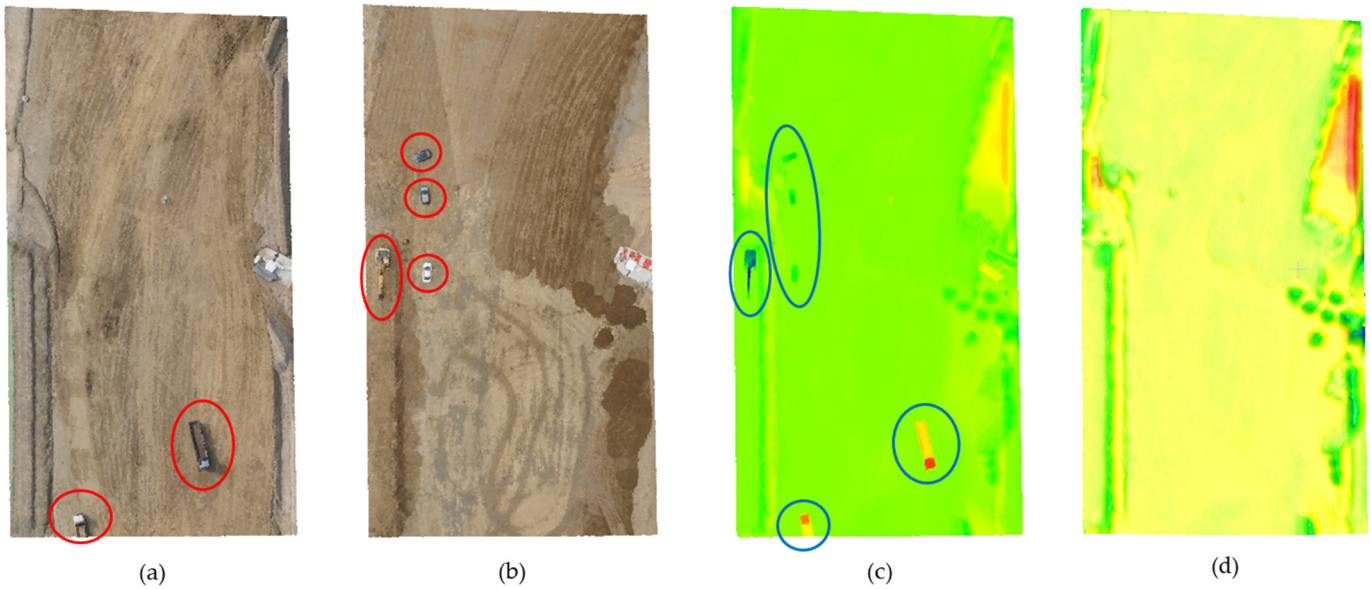

Figure 12. The effect of moving objects on the height differential map. (**a**,**b**) represent moving objects in the original point clouds collected from Round 1 and Round 2, respectively; (**c**) illustrates the errors in the original differential map; and (**d**) shows the differential map without moving objects.

Recently, with the advancement of deep learning technologies, various methods for classifying and segmenting specific objects in 3D point cloud data have been proposed [38,39]. However, there are a few 3D datasets containing construction objects to train deep learning models. Even though some studies introduced 3D construction object datasets that include construction equipment [40,41], they were made by terrestrial laser scanning, which is quite different from that produced by UAS. For this reason, this study could not apply methods that can automatically segment construction objects in 3D point clouds. For further research, we are now constructing a UAS-generated 3D dataset that includes various construction objects. We expect that the next version of the earthwork progress digitalization system can be fully automated by eliminating the manual process of erasing moving objects in 3D point clouds.

5. Conclusions

This study presents an all-in-one framework for large-scale earthwork progress digitalization using a series of 3D models generated from UAS images. The entire process of the framework includes precise 3D topographic model generation, model quality control, earthwork volume estimation, cross-section view generation, and geofencing drawing. The developed earthwork data processing system was validated by a case study from an

active highway construction site. By examining the case study, we identified that highly precise 3D topographical maps can be created by UAS images, and the 3D maps can be actively used for volume change estimation and earthwork progress documentation. Moreover, the developed system was able to draw geofencing onto 3D models, which can be used for safe operation and transportation of heavy equipment. We expect that the proposed framework can contribute to smart construction areas by automating the process of digitizing earthwork.

As discussed, a major limitation of the proposed practices is that this system needs manual preprocessing to remove outliers in 3D point clouds caused by moving objects, such as construction equipment, cars, or workers. These objects can cause significant errors when estimating volume changes or creating geofencing. In future studies, therefore, we will investigate a method of automatically removing non-construction objects to build precise 3D topo models. Another drawback of this study is that a rather small number of GCPs were used for georeferencing because the site where we acquired the data was an active construction site. Although the positioning errors of 3D point clouds measured in this study were less than 3 cm in the horizontal direction and 4 cm in the vertical direction, these errors could be further reduced if more GCPs were used. Thus, in future studies, a larger number of GCPs can be installed by conducting prior consultation with the construction field managers.

Author Contributions: Conceptualization, J.-K.L. and J.-W.C.; methodology, J.-K.L.; software, J.P.; validation, J.-K.L. and J.-W.C.; formal analysis, J.P.; investigation, J.-W.C.; resources, J.-W.C.; data curation, J.-K.L.; writing—original draft preparation, J.-W.C.; writing—review and editing, J.-K.L. and J.P.; visualization, J.P.; supervision, J.-K.L.; project administration, J.-W.C.; funding acquisition, J.-K.L. All authors have read and agreed to the published version of the manuscript.

Funding: This research was funded by the Korea Agency for Infrastructure Technology Advancement under the Ministry of Land, Infrastructure and Transport, grant number (No.2 1SMIP-A158708-02).

Institutional Review Board Statement: Not applicable.

Informed Consent Statement: Not applicable.

Data Availability Statement: Not applicable.

Acknowledgments: This research was conducted with the support of the "National R&D Project for Smart Construction Technology (No.2 1SMIP-A158708-02)" funded by the Korea Agency for Infrastructure Technology Advancement under the Ministry of Land, Infrastructure and Transport, and managed by the Korea Expressway Corporation.

Conflicts of Interest: The authors declare no conflict of interest.

References

1. Štefanič, M.; Stankovski, V. A review of technologies and applications for smart construction. In *Proceedings of the Institution of Civil Engineers-Civil Engineering*; Thomas Telford Ltd.: London, UK, 2018; pp. 83–87.
2. Liu, D.; Lu, W.; Niu, Y. Extended technology-acceptance model to make smart construction systems successful. *J. Constr. Eng. Manag.* **2018**, *144*, 4018035. [CrossRef]
3. Azar, E.R.; Kamat, V.R. Earthmoving equipment automation: A review of technical advances and future outlook. *J. Inf. Technol. Constr.* **2017**, *22*, 247–265.
4. Han, S.-W.; Lee, S.-Y.; Halpin, D.W. Productivity evaluation of the conventional and GPS-based earthmoving systems using construction simulation. In Proceedings of the Construction Research Congress 2005: Broadening Perspectives, San Diego, CA, USA, 5–7 April 2005; pp. 1–9.
5. Kim, S.-K.; Min, S.-G. Development of a work information model and a work path simulator for an intelligent excavation. *J. Korean Soc. Civ. Eng.* **2012**, *32*, 259–267.
6. Park, J.S.; Seo, J.W. Application of Construction Equipment Fleet Management System through the Case Study of Air and Vessel Traffic Control Technology. *J. Korean Soc. Civ. Eng.* **2015**, *35*, 493–500. [CrossRef]
7. Gwak, H.-S.; Seo, J.-W.; Lee, D.-E. Earthmoving haul-route searching method for energy saving based on evolutionary algorithm. *J. Archit. Inst. Korea Struct. Constr.* **2015**, *31*, 81–88. [CrossRef]
8. Park, J.; Kim, S. Productivity analysis for the 3D digitization of earthwork sites based on scanning conditions. *Int. J. Railw.* **2018**, *11*, 1–9.

9. Kim, S.; Irizarry, J.; Costa, D.B. Potential factors influencing the performance of unmanned aerial system (UAS) integrated safety control for construction worksites. In Proceedings of the Construction Research Congress 2016, San Juan, PR, USA, 31 May–2 June 2016; pp. 2614–2623.
10. Gupta, L.; Jain, R.; Vaszkun, G. Survey of important issues in UAV communication networks. *IEEE Commun. Surv. Tutor.* **2015**, *18*, 1123–1152. [CrossRef]
11. Rangel, J.M.G.; Gonçalves, G.R.; Pérez, J.A. The impact of number and spatial distribution of GCPs on the positional accuracy of geospatial products derived from low-cost UASs. *Int. J. Remote Sens.* **2018**, *39*, 7154–7171. [CrossRef]
12. Oniga, V.-E.; Breaban, A.-I.; Pfeifer, N.; Chirila, C. Determining the Suitable Number of Ground Control Points for UAS Images Georeferencing by Varying Number and Spatial Distribution. *Remote Sens.* **2020**, *12*, 876. [CrossRef]
13. Ronchi, D.; Limongiello, M.; Barba, S. Correlation among Earthwork and Cropmark Anomalies within Archaeological Landscape Investigation by Using LiDAR and Multispectral Technologies from UAV. *Drones* **2020**, *4*, 72. [CrossRef]
14. Hanna, A.; Hintz, C.; Vonderohe, A. *3D Design Terrain Models for Construction Plans and GPS Control of Highway Construction Equipment*; CFIRE: Madison, WI, USA, 2010.
15. Lee, J.K.; Park, J.S.; Roberts, G.W.; Oluropo, O.; Moon, D.J. Study on Issues of Tilt-meters and Utilization of GPS in Bridge Monitoring System (BMS). In Proceedings of the Joint International Symposium on Deformation Monitoring, Hong Kong, China, 2–4 November 2011; pp. 2–4.
16. Dampegama, K.P.; Abesinghe, A.; Dinusha, K.A.; Vandebona, R. Comparative Study on Methods For 3D Modelling with Traditional Surveying Technique and Total Station Technique. In Proceedings of the 11th International Research Conference, Rathmalana, Sri Lanka, 13–14 September 2018.
17. Slattery, K.T.; Slattery, D.K.; Peterson, J.P. Road construction earthwork volume calculation using three-dimensional laser scanning. *J. Surv. Eng.* **2012**, *138*, 96–99. [CrossRef]
18. Williams, K.E. Accuracy Assessment of LiDAR Point Cloud Geo-Referencing. Master's Thesis, Oregon State University, Corvallis, OR, USA, June 2012.
19. Cho, Y.K.; Park, J. *Assessment of Construction Points for Grade Control and Reference in 3D*; Georgia Dept. of Transportation: Atlanta, GA, USA, 2018. Available online: http://g92018.eos-intl.net/eLibSQL14_G92018_Documents/16-18.pdf (accessed on 10 November 2021).
20. Kim, S.; Irizarry, J.; Costa, D.B. Field Test-Based UAS Operational Procedures and Considerations for Construction Safety Management: A Qualitative Exploratory Study. *Int. J. Civ. Eng.* **2020**, *18*, 919–933. [CrossRef]
21. Park, J.; Kim, P.; Cho, Y.K. Automated collaboration framework of UAV and UGV for 3D visualization of construction sites. In Proceedings of the 18th International Conference on Construction Applications of Virtual Reality, Auckland, New Zealand, 22–23 November 2018.
22. Kim, P.; Price, L.C.; Park, J.; Cho, Y.K. UAV-UGV Cooperative 3D Environmental Mapping. In Proceedings of the ASCE International Conference on Computing in Civil Engineering 2019: Data, Sensing, and Analytics, Atlanta, GA, USA, 17–19 June 2019; pp. 384–392. [CrossRef]
23. Wang, X.; Al-Shabbani, Z.; Sturgill, R.; Kirk, A.; Dadi, G.B. Estimating earthwork volumes through use of unmanned aerial systems. *Transp. Res. Rec.* **2017**, *2630*, 1–8. [CrossRef]
24. Kavaliauskas, P.; Židanavičius, D.; Jurelionis, A. Geometric Accuracy of 3D Reality Mesh Utilization for BIM-Based Earthwork Quantity Estimation Workflows. *ISPRS Int. J. Geo-Inf.* **2021**, *10*, 399. [CrossRef]
25. Jeong, I.; Jang, Y.; Park, J.; Cho, Y.K. Motion Planning of Mobile Robots for Autonomous Navigation on Uneven Ground Surfaces. *J. Comput. Civ. Eng.* **2021**, *35*, 4021001. [CrossRef]
26. Kim, P.; Park, J.; Cho, Y.K. As-is geometric data collection and 3D visualization through the collaboration between UAV and UGV. In Proceedings of the International Symposium on Automation and Robotics in Construction (ISARC 2019), Banff, AB, Canada, 21–24 May 2019. [CrossRef]
27. Mandirola, M.; Casarotti, C.; Peloso, S.; Lanese, I.; Brunesi, E.; Senaldi, I.; Risi, F.; Monti, A.; Facchetti, C. Guidelines for the use of Unmanned Aerial Systems for fast photogrammetry-oriented mapping in emergency response scenarios. *Int. J. Disaster Risk Reduct.* **2021**, *58*, 102207. [CrossRef]
28. Calantropio, A.; Chiabrando, F.; Sammartano, G.; Spanò, A.; Losè, L.T. UAV Strategies Validation and Remote Sensing Data for Damage Assessment in Post-Disaster Scenarios. In Proceedings of the International Archives of the Photogrammetry, Remote Sensing and Spatial Information Sciences, Istanbul, Turkey, 18–21 March 2018; pp. 121–128.
29. Chiabrando, F.; Giulio Tonolo, F.; Lingua, A. *UAV Direct Georeferencing Approach in an Emergency Mapping Context. The 2016 Central Italy Earthquake Case Study*; International Society for Photogrammetry and Remote Sensing: Enschede, The Netherlands, 2019.
30. Orych, A. Review of methods for determining the spatial resolution of UAV sensors. *Int. Arch. Photogramm. Remote Sens. Spat. Inf. Sci.* **2015**, *40*, 391–395. [CrossRef]
31. Lee, T.Y. Spatial Resolution Analysis of Aerial Digital Camera. Ph.D. Thesis, Dong-A University, Busan, Korea, 2012.
32. Lee, J.; Sung, S. Evaluating spatial resolution for quality assurance of UAV images. *Spat. Inf. Res.* **2016**, *24*, 141–154. [CrossRef]
33. Zhou, Q.-Y.; Park, J.; Koltun, V. Open3D: A modern library for 3D data processing. *arXiv* **2018**, arXiv:1801.09847. Available online: https://arxiv.org/abs/1801.09847v1 (accessed on 10 November 2021).
34. Rusu, R.B.; Cousins, S. 3D is here: Point Cloud Library (PCL). In Proceedings of the 2011 IEEE International Conference on Robotics and Automation, Shanghai, China, 9–13 May 2011.

35. Zhang, Z. Iterative point matching for registration of free-form curves and surfaces. *Int. J. Comput. Vis.* **1994**, *13*, 119–152. [CrossRef]
36. Gonzalez, M.; Luaces, A.; Dopico, D.; Cuadrado, J. A 3d physics-based hydraulic excavator simulator. In Proceedings of the ASME World Conference on Innovative Virtual Reality, Chalon-sur-Saône, France, 25–26 February 2009; pp. 75–80.
37. Ni, T.; Zhang, H.; Yu, C.; Zhao, D.; Liu, S. Design of highly realistic virtual environment for excavator simulator. *Comput. Electr. Eng.* **2013**, *39*, 2112–2123. [CrossRef]
38. Qi, C.R.; Su, H.; Mo, K.; Guibas, L.J. PointNet: Deep learning on point sets for 3D classification and segmentation. In Proceedings of the IEEE Conference on Computer Vision and Pattern Recognition, Honolulu, HI, USA, 21–27 July 2017; pp. 77–85. [CrossRef]
39. Qi, C.R.; Yi, L.; Su, H.; Guibas, L.J. PointNet++: Deep hierarchical feature learning on point sets in a metric space. *arXiv* **2017**, arXiv:1706.02413. Available online: https://arxiv.org/abs/1706.02413 (accessed on 10 November 2021).
40. Park, J.; Cho, Y.K. Point Cloud Information Modeling: Deep Learning–Based Automated Information Modeling Framework for Point Cloud Data. *J. Constr. Eng. Manag.* **2022**, *148*, 4021191. [CrossRef]
41. Park, J.; Chen, J.; Cho, Y.K. Point Cloud Information Modeling (PCIM): An Innovative Framework for as-is Information Modeling of Construction Sites. In Proceedings of the Construction Research Congress 2020: Computer Applications, Tempe, AZ, USA, 8–10 March 2020; pp. 1319–1326. [CrossRef]